Theses and Dissertations

2018

# Development of a High-Resolution Spatial Heterodyne Libs Spectrometer

Kevin A. Dudley
*University of South Carolina*

Follow this and additional works at: https://scholarcommons.sc.edu/etd

Part of the Chemistry Commons

DEVELOPMENT OF A HIGH-RESOLUTION SPATIAL HETERODYNE LIBS
SPECTROMETER

by

Kevin A. Dudley

Bachelor of Science
Fairmont State University, 2016

Submitted in Partial Fulfillment of the Requirements

For the Degree of Master of Science in

Chemistry

College of Arts and Sciences

University of South Carolina

2018

Accepted by:

Stanley M. Angel, Director of Thesis

John Ferry, Reader

Cheryl L. Addy, Vice Provost and Dean of the Graduate School

## DEDICATION

First and foremost, I would like to thank my Lord and Savior who has been my guide throughout my life journey. Equally important, I want to thank my loving and supporting wife. Without her encouragement, patience, love, and dedicated support, the accomplishments I have made would not be possible. Thank you to my children who have been the most amazing children because of their understanding and patience while working to further my education. Finally, my father and late mother who have been my rock throughout my life. He continues to give me unending support no matter which direction I turn in my life and his patience and love have never wavered. She always did and continues to inspire me with words she told me as a child, "You can do anything you want to do as long as you set your mind to it.

# ACKNOWLEDGEMENTS

ABSTRACT

Laser-Induced Breakdown Spectroscopy (LIBS) is an atomic emission technique

that uses a pulse laser to ablate a sample and form a plasma. Atomic emissions from the

plasma provide unique elemental characteristics regarding the composition of the sample.

The technique produces valuable qualitative results, but the accuracy of quantitative

analyses is hindered by spectral line broadening mechanisms and laser pulse

reproducibility, among other factors. The Spatial Heterodyne Spectrometer (SHS) is a

high-resolution spectrometer with very high light throughput, and its use to LIBS is

currently limited to two peer-reviewed publications. In the following work a high

resolution SHS is developed and explored for LIBS measurements of isotopes.

# TABLE OF CONTENTS

# LIST OF FIGURES

viii

# LIST OF ABBREVIATIONS

CCD ................................................................................Charge-Coupled Device

DOE ................................................................................Department of Energy

FWHM ............................................................................Full-Width at Half-Maximum

HeNe ..............................................................................Helium Neon

IAEA ..............................................................................International Atomic Energy Agency

iCCD ..............................................................................intensified Charge-Coupled Device

ICP-MS ..........................................................................Inductively-Coupled Plasma-Mass Spectrometry

ICP-OES .........................................................................Inductively-Coupled Plasma-Optical Emission Spectrometry

IR....................................................................................Infrared

LAMIS ...........................................................................Laser Ablation Molecular Isotope Spectrometry

LIBS ...............................................................................Laser-Induced Breakdown Spectroscopy

LIP..................................................................................Laser-Induced Plasma

MS..................................................................................Mass Spectrometry

Nd:YAG..........................................................................Neodymium: Yttrium Aluminum Garnet

NIR.................................................................................Near Infrared

Ro-Vib............................................................................Rotational-Vibrational

SHIMMER .....................................................................Spatial Heterodyne Imager for Mesospheric Radicals

SHLS ..............................................................................Spatial Heterodyne LIBS Spectrometer

SHS ................................................................................Spatial Heterodyne Spectrometer

S/N .................................................................................Signal-to-Noise Ratio

CHAPTER 1

REVIEW OF LASER-INDUCED BREAKDOWN SPECTROSCOPY

1.1 INTRODUCTION TO LASER-INDUCED BREAKDOWN SPECTROSCOPY

Laser-induced breakdown spectroscopy (LIBS) is an atomic emission technique that uses a high-power laser beam focused onto a sample with an irradiance of more than one $GW/cm^2$ at the focal point. Initially, the sample is ablated followed by the formation of an overall electrically neutral plasma, ideally with the same elemental chemical composition as the ablated material from the sample. [1] The plasma provides photo and thermal excitation of the atoms, ions, and molecules producing an emission continuum due to Bremsstrahlung and recombination events after which atomic/ionic and molecular emission occur. [1] Figure 1.1 shows a LIBS energy level diagram showing the excitation and emission events during the evolution of the plasma. Bremsstrahlung emission is created by free electrons emitting a photon due to acceleration and deceleration initiated by inelastic collisions with other particles. Recombination emission is from photons being emitted during the loss of kinetic energy when free electrons recombine with ionized species. Atomic/ionic emission is due to the element-dependent transitions between the electronic states and thus provides unique fingerprints for each emitting species. Molecular emission occurs after the plasma cools sufficiently to allow molecules to form and are often radical species. The plasma temperature is still very high during this period and continues to thermally excite atoms and molecules. [1,3] The atomic, ionic, and/or molecular emission signals can be detected using time-resolved methods as the

1

plasma cools. [1] Continuum emission decays at a much faster rate (fs) than the atomic emission (ns) leaving a window for detection of elemental spectral lines using gated detection. [1,2]

LIBS measurements require only line-of-sight to the sample and no sample preparation. [4,5] The non-invasive characteristic of the technique offers the capability to make remote, in-situ chemical measurements in extreme environments. Drawbacks of the technique are low sensitivity, poor shot-to-shot reproducibility, and spectral line broadening effects due to plasma-sample interactions. [1] Poor reproducibility is due to variability in laser power, atmospheric conditions, laser beam shape, spot size, and/or position of the ablation point (which becomes critical at standoff distances). [6,7] Many studies aimed at increasing the sensitivity and overcoming matrix effects produced by plasma-sample interactions that cause the broadening mechanisms have been investigated. [1,8,9] Plasma properties causing spectral line broadening are discussed later in the section describing plasma formation, and line broadening is the primary reason measurements of isotopes using LIBS is difficult. However, recent research by D'Ulivo et al has shown that successful qualitative and quantitative measurements of chemical compositions of isotopes are possible. [10]

## 1.2 LIBS INSTRUMENT DESIGN

The general instrument design for LIBS has five components as shown in Figure 1.2 and are as follows: high-power pulsed-laser, focusing optics, collection optics, spectrometer, and a gated detector. The pulsed-laser is commonly a neodymium yttrium aluminum garnet (Nd: YAG) laser operating at the 1064 nm fundamental or frequency-doubled wavelength (532 nm) with nanosecond pulse-widths or titanium:sapphire lasers

2

operating typically around 800 nm (range from 600 nm – 1100 nm) at femtosecond pulse-widths. [11] The focusing optics are generally a simple lens positioned such that the focal point of the lens is at or just below the surface of the sample for solid samples. For liquids, the focus can be on the surface or inside the sample. In systems setup for back-collection, the focusing optics serve as the collection optics. The collected signals are directed into the entrance aperture of the spectrometer where the wavelengths are separated and sent to the detector.

## 1.3 LASER-INDUCED PLASMA (LIP) FORMATION

Plasma formation is a multi-photon process that is initiated by the high irradiance at the focal point which provides enough energy to ablate a small portion of the sample. As the ejecta from the ablation point is bombarded with more photons, a plasma forms reaching temperatures greater than 15,000 K. [1] The plasma has an overall neutral charge but contains localized area with a high density of free electrons and ionized atoms which produce locally strong electric fields throughout the plasma. The electric fields cause splitting of normally degenerate energy levels, known as the Stark effect. The Stark effect, commonly referred to as Stark broadening of atomic emission lines, is similar to the Zeeman effect caused by strong magnetic fields. [12,13] The splitting of the electronic degeneracies produce line broadening in atomic spectral lines that can be on the order of hundreds of picometers. [1] Doppler broadening also occurs within the LIP when the emitting species is moving away from or toward the detector. Doppler broadening can be on the order of tens of picometers. [1]

3

## 1.4 LIBS APPLICATIONS

Qualitative and quantitative applications of LIBS have expanded due to advances in technology and growing desire for portable instrumentation. [2,8] LIBS techniques have been explored for elemental, isotopic, and molecular analyses for applications in planetary exploration, [1,14,15] nuclear material proliferation, [8] and explosives detection. [4,16,17] Other fields where a significant interest in LIBS techniques is growing are industrial materials processes, agriculture, ecology, biology, biomedical, geochemistry, forensics, and cultural heritage. [1,6,8,9,18,19]

Planetary research and exploration can benefit greatly from the ability to make remote chemical measurements in extreme environments in real time. The ChemCam LIBS instrument currently onboard the Mars Curiosity Rover has successfully demonstrated the effectiveness of remote LIBS and defines LIBS as a valuable tool in planetary exploration. [14,15] With recent terrorist threats to the military and civilian populations, LIBS techniques have been developed for explosives detection. [4,16,17] Agricultural LIBS applications include pH measurements and trace metal soil analysis. [8] For industrial applications, LIBS measurements are used for in-situ quality assurance in the production of bulk materials. [8]

LIBS has received much attention in the nuclear proliferation field and proves to be a much-needed asset for investigators provided reproducibility and quantification issues are resolved. [3] LIBS measurements are generally associated with atomic emission but in recent years applications in molecular emission such as laser ablation molecular isotope spectrometry (LAMIS) have been explored. LAMIS is basically LIBS measurements of molecular emissions using longer gate delays. [3]

4

Using the innovative spatial heterodyne spectrometer (SHS), LIBS has the potential to provide remote, in-situ, multi-element and isotopic chemical measurements for investigation of nuclear materials and beyond. The SHS was first described by Harlander and is an interferometer like the Michelson interferometer but uses fixed gratings tilted to a specific angle dictated by a user-defined Littrow wavelength. All other wavelengths heterodyne about the Littrow wavelength producing high-resolution spectra with the benefit of high-throughput. [20]
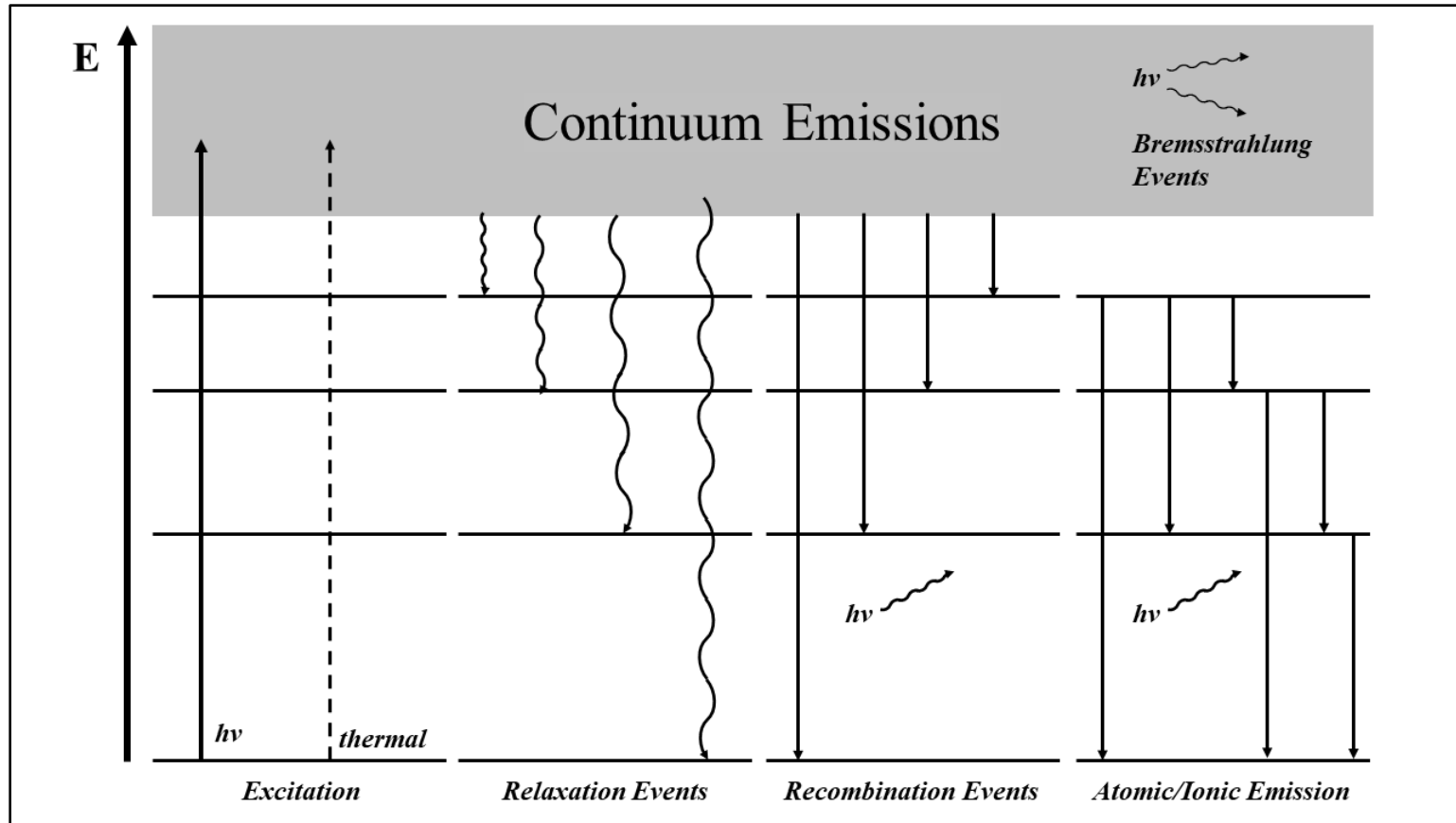
Figure 1.1 The figure illustrates a LIBS energy level diagram for the excitation and emission transitions during the evolution of the LIP. From left to right, photo or thermal excitation occurs, (top) Bremsstrahlung emission, non-emissive relaxation transitions, recombination events, and atomic/ionic emissions.
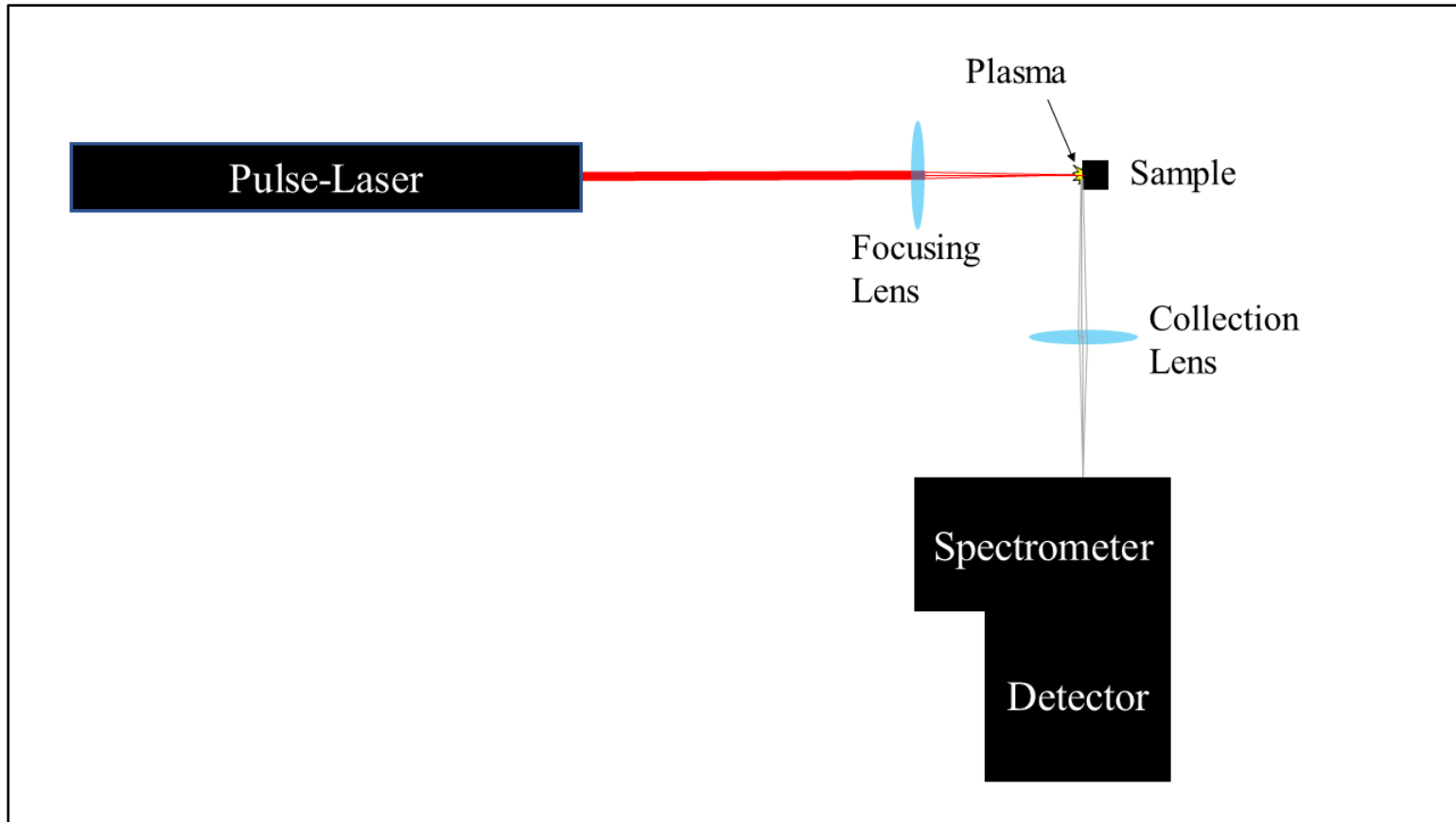
Figure 1.2 General layout scheme for LIBS. The collection lens is oriented in the orthogonal position but is often placed behind a dichroic mirror for 180-degree collection of LIBS signals.

# CHAPTER 2

# ISOTOPE MEASUREMENTS USING OPTICAL EMISSION

## 2.1 ISOTOPE MEASUREMENTS FOR NUCLEAR PROLIFERATION

Isotope measurements are important for nuclear proliferation and material dating. Nuclear safeguard inspections mandated by the Department of Energy (DOE) and International Atomic Energy Agency (IAEA) require the ability to measure U and Pu isotope ratios. [3,10,21,22] The isotopic spectral line shift for the 424.4 nm emission line of $^{235}U/^{238}U$ is ~25 pm, for the 594.5 nm emission line of $^{239}Pu/^{240}Pu$ it is ~6 pm, and for $^{6}Li/^{7}Li$ at 670.8 nm it is ~15 pm. [2,21,22] Optical separation and detection of the small isotopic shifts in spectral emission lines are challenging for any high-resolution instruments and even more so for LIBS measurements because the magnitude of spectral emission line broadening can be an order or two larger than the isotopic emission line shifts.

The most well-known and well-established techniques for measuring isotope ratios are mass spectrometry (MS) methods such as thermal-ionization-MS (TIMS) and inductively-coupled plasma-MS (ICP-MS). The extremely high mass accuracy of MS techniques makes it ideal for isotopic measurements because each isotope has a distinct mass and the chemical properties of the isotopes are so similar that matrix effects are generally insignificant. [23] High-resolution MS instruments are expensive, large, and often require complex sample preparation. A portable instrument capable achieving high-

resolution isotopic measurements would be a considerable asset to nuclear site investigators. [2,3]

## 2.2 ISOTOPE MEASUREMENT INSTRUMENTS AND METHODS

Optical techniques used to measure isotope emission include inductively-coupled-plasma optical emission spectrometry (ICP-OES), laser ablation molecular isotope spectrometry (LAMIS), and LIBS. Molecular rotational-vibrational (Ro-Vib) analytical techniques such as Raman and infrared (IR) are sensitive to the change in mass with regards to isotopes but only provide primarily molecular information or with limited elemental information.

Krachler et al developed an analytical method to determine the production age of Pu materials using a commercially available ICP-OES instrument to measure isotope ratios of $^{234}$U and $^{238}$Pu. The group was able to achieve spectral resolution less than 5 pm. [24] The procedure also allowed for a direct measurement of the isotope emission lines for the $^{234}$U and $^{238}$Pu simultaneously without requiring chemical separation of the two analytes normally required for MS. ICP-OES allows multi-element detection but requires a clean laboratory environment and sample preparation.

A recently described laser ablation technique called LAMIS has been used to measure numerous isotope ratios. [3,8,21,22] LAMIS is similar to LIBS in that emission is measured following laser ablation, however, LAMIS requires long gate delay times to allow elements to recombine or combine with oxygen or other atmospheric elements to form molecules. The newly formed molecules are thermally excited within the plasma producing molecular Ro-Vib emission bands that are sensitive to element mass. [25] Molecular isotope shifts are considerably larger than electronic isotope shifts so only

9

moderately high-resolution is required to resolve peaks. [2,24] One drawback of the method is that only one element can be analyzed per acquisition. An instrument with the same capabilities as LAMIS instruments that can measure a broader range of elements would be ideal.

Despite broadening of elemental spectral emission lines, LIBS spectroscopy has been successfully demonstrated for elemental, isotopic, and molecular analyses and can do so without the use of a vacuum chamber or carrier gases like many current methods used for high resolution elemental analysis. [1-3,10] Markushin et al quantitatively characterized D/H ratios in protein using LIBS. [9] D'Ulivo et al have investigated ratios of D/H in gas reaction products and reported isotopic resolution for the Balmer emission line of D/H (~656 nm) with a separation of ~180 pm despite the Stark broadening of the emission lines. [10] Cremers et al were able to measure and resolve $^6Li/^7Li$ with a handheld LIBS unit and high-resolution Echelle spectrometers (6.8 pm – 10.0 pm resolution). [2]

Line widths for LIBS spectra are generally hundreds of picometers at atmospheric pressure making resolution of most elemental isotopic emission line shifts extremely difficult. [2] Long gate delay times allow plasma expansion, thermal emission, and electron density to decay to levels below the intensity of the atomic emission lines. [10] Stark broadening would be significantly reduced with a lower electron density and weaker electric field producing a window of opportunity where full-width at half-maximum (FWHM) may be less than elemental isotopic line separations. While atomic emission decays with the plasma it does so at a slower rate. A high-throughput spectrometer would be able to take advantage of the window during long gate delays.

# CHAPTER 3

# HIGH-RESOLUTION SPATIAL HETERODYNE LIBS
# SPECTROMETER (SHLS)

## 3.1 THE SPATIAL HETERODYNE LIBS SPECTROMETER (SHLS)

The SHS was first described by Harlander. [26] The SHS is similar to a Michelson

interferometer but uses tilted, stationary diffraction gratings in lieu of mirrors. This gives

the SHS a huge advantage over other high-resolution spectrometers since it has no

moving parts. The schematic and working principle of the SHS can be seen in Figure 3.1.

The angle of tilt is dictated by the Littrow wavelength which is a user-defined wavelength

that is retroreflected with respect to the optical axis and produces no interference pattern

upon recombination. All other wavelengths are diffracted at wavelength-specific angles

from the optical axis and produce crossing wave-fronts at the beam-splitter to form a

wavenumber-dependent interference pattern that is heterodyned around the Littrow

wavenumber. The heterodyne interference pattern allows for high spectral resolution with

a limited number of detector elements. The SHS has no moving parts and is thus,

compatible with gated detection. [20]

The SHS design is compatible with a broad range of wavelengths ranging from

the ultraviolet (UV) to the near infrared (NIR). [26-28] The two SHS gratings are tilted at

angle $\theta_L$, the Littrow angle, so that one wavelength is retroreflected and can be calculated

using the grating equation (1).

$$m \cdot \lambda_L = d \cdot (\sin \alpha + \sin \beta) \qquad (1)$$

In this equation $m$ is the grating order, $\lambda_L$ is the user-defined Littrow wavelength and $d$ is the distance between the grooves on the grating. [26-28] In the case of the Littrow condition, the angle of incidence ($\alpha$) is equal to the angle of reflection ($\beta$) so the equation becomes (2):

$$m \cdot \lambda_L = 2d \cdot \sin\theta_L \tag{2}$$

All other wavelengths are heterodyned about the Littrow wavelength creating a wavelength dependent fringe pattern upon recombination at the beam-splitter. The Fourier transform of the interferogram yields the frequency spectrum.

The number of fringes (f) at a selected wavenumber is related to the Littrow wavelength by equation (3):

$$f = 4 \cdot (\sigma - \sigma_L) \cdot \tan\theta_L \tag{3}$$

In equation # $\sigma$ is the wavenumber of interest and $\sigma_L$ is Littrow in wavenumbers. [26-28] Wavenumbers above and below Littrow produce the same fringe patterns and thus, overlap on the detector, as shown by the degeneracy in equation (3). By cross-tilting one of the gratings vertically, the fringes above and below Littrow are rotated in opposite directions and both can be recovered without ambiguity using a 2D Fourier Transform. [20]

The resolving power (R) of the SHS is equal to the number of grooves illuminated on the gratings as shown in equation (4):

$$R = 2 \cdot w \cdot d = \frac{\lambda_L}{\Delta\lambda} \tag{4}$$

In equation 4 $w$ is the grating width, $d$ is the groove density, $\lambda_L$ is the Littrow wavelength, and $\Delta\lambda$ is the resolution (FWHM). [26-28] The spectral range ($SR$) is inversely proportional to resolving power ($R$) as shown in equation (5):

$$SR = \frac{N \cdot \lambda}{2 \cdot R} \tag{5}$$

where N is the number of horizontal pixels on the detector. [26-28]

The first use of the SHS for active spectroscopy was described by Gomer et al for Raman spectroscopy. [29] The first spatial heterodyne LIBS spectrometer (SHLS) was described by Gornushkin et al [30] followed by a standoff version described by Barnett et al for LIBS measurements up to 20 m. [20] The high-throughput and spectral resolution offers the potential for high resolution LIBS measurements while maintaining high optical throughput. The resolution of the SHLS combined with its wavelength precision and stability should allow more precise measurement and resolution of elemental isotope spectral emission.

## 3.2 EXPERIMENTAL SETUP

The high resolution SHLS uses a Continuum Surelite SLII-10 (Continuum, San Jose, CA, USA) Nd:YAG pulsed-laser operating at the fundamental wavelength with power of ~10 – 15 mJ per pulse with a pulse-width of ~7 ns. The laser beam was focused onto the sample using an f/2 planoconvex lens with antireflective coating. Fine tuning of the focal point was achieved by mounting the focusing lens to a x-y translational stage. The same type of lens was used for the collection and was placed such that the focal point was overlapped with the focal point of the focusing lens. Two 25 mm irises were used to define the entrance aperture of the SHS and to minimize the amount of off-axis light collected. The SHS was constructed as shown in Figure 3.2 with 25 mm x 25 mm 300 or 600 grooves/mm diffraction gratings blazed at 500 nm and Thor Labs Model BS013 25 mm non-polarizing 50:50 cube beam-splitter. The diffraction gratings were mounted to x-y translational stages and a micrometer-adjusted rotational stage for fine-tuning the grating angle and distance. A Nikon AF Micro Nikkor f/2.8 105 mm camera lens was

13

used to image the face of the diffraction gratings onto a Princeton Instruments PI-MAX 1024 x 256 pixel thermoelectrically-cooled, intensified charge-coupled device, or iCCD, (Princeton Instruments, Trenton, NJ) with 26 μm pixel size. The iCCD gate timing parameters for LIBS measurements of copper were 1.5 μs for the delay and 10.5 μs for the width with a gain of 255 to measure LIBS signals and helium-neon (HeNe) lamp to maximize signal-to-noise. The imaging lens was positioned such that the diffraction gratings and iCCD were two focal lengths away to give unity magnification. The illuminated portion of the gratings was ~22 mm which just slightly over-filled the intensified portion of the CCD when imaged into the detector. Copper samples (unknown purity) measured with the SHLS were obtained from an industrial supply company. [20]

3.2 RESULTS AND DISCUSSION

The SHS was aligned by aiming the Thor Labs 532 nm alignment laser through the center of the entrance face of the beam-splitter and measuring the height of the transmitted and reflected beams. The tilts of the beam-splitter mount were adjusted such that the back reflection from the beam-splitter retroreflected and the transmitted and reflected laser beams were at the exact same height as the beam at the exit port of the alignment laser. The zero-path difference (ZPD) between the diffraction gratings was achieved by measuring the distance between the face of each grating and the center of the beam-splitter using a ruler. The ZPD was fine-tuned by shining white light into the SHS and adjusting the distance using the translation stage micrometer and vertical grating tilt until vertical white-light fringes were observed from the output of the SHS. The white light fringes indicate that the ZPD is within 10 nm which is about the coherence length of white light.

14

The initial Littrow wavelength was set to 532 nm using a Thor Labs green alignment laser. The gratings were rotated such that the first order from each grating overlapped and produced a fringe pattern with only one to two vertical fringes were visible. For measuring a low-pressure mercury lamp, the gratings were rotated by adjusting the micrometer-actuated rotation in 1 μm increments to increase the Littrow wavelength to ~544 nm. To accomplish this an Ocean Optics HG-1 reference lamp was directed into the SHS and a measurement was made after each adjustment until a fringe pattern from the 546 nm Hg emission line appeared. To verify the Littrow setting, the actual Littrow was calculated using the fringe equation (equation 3) where σ is the wavenumber for the 546 nm line and $\theta_L$ is calculated using the grating equation and estimating $\lambda_L$ as 544 nm. The fringes/cm can be obtained from the number of fringes/pixel on the charge-coupled device (CCD) divided by the width of each pixel. An image of the fringe pattern used to count the number of fringes over a pixel range is shown in figure 3.3. The fringes/cm can be obtained from a cross-section plot of the interference pattern shown in figure 3.4. Simply count the number of peaks over a specific range of pixels and divide that number by the product of the specific pixel range times pixel size.

A calibration curve was made to set the SHS to a specific Littrow wavelength simply based on the micrometer settings on the rotational stages. The calibration curve (in Figure 3.5) has a slope of 1.312 ±0.004 μm/nm and a y-intercept of 532.85 ±0.1 nm both calculated using the linear regression algorithm in Microsoft Excel. Using the regression line from the calibration curve the Littrow can be set to any wavelength by the appropriate rotation stage settings. This was how the SHLS was switched back and forth

15

to measure Cu LIBS or the mercury lamp. To verify the accuracy of the calibration method, Littrow was set to 532 nm and the required adjustment was made to successfully measure the 521 nm Cu emission line. Likewise, the Littrow was set and adjusted to successfully measure the 576 nm and 579 nm mercury emission lines.

To test the resolution of the SHS, measurements of the 546 nm, 576 nm, and 579 nm mercury emission lines were made in two ways. First, using the 300 groove/mm gratings, the second order from gratings increases the resolving power of the SHS two-fold. The resolution of the 546 nm mercury emission line using the first order of those gratings was 108 pm determined by measuring the FWHM of the 546 nm mercury line shown in Figure 3.6. The theoretical resolving power of this system is 15,000. The resolution achieved was 5056 with a spectral range of 22.7 nm for the first order measurements. The gratings were simultaneously rotated to measure the same emission line using the second order and a resolution of 61.1 pm was achieved as shown in Figure 3.7. The expected resolution should have been half that of the first-order since the resolving power was doubled. The actual resolution using the second order was 8936 with a spectral range of 6.3 nm which is considerably lower than two-times the expected resolution and less than half the expected spectral range. One reason for the loss of resolution may be due to the lack of filters in the system to block out higher orders from lower wavelengths which may reduce resolution. Finally, the diffraction gratings were exchanged for 600 groove/mm gratings blazed at 500 nm which has the same resolving power as the second order previously mentioned. Measuring the mercury lamp with the new system produced a resolution for the 546 nm mercury emission line of 58.2 pm with a spectral range of 9.6 nm meaning that the actual resolution with the 600 groove/mm

gratings was 9383 which is nearly double that with the 300 gr/mm gratings in first order. The spectrum is shown in Figure 3.8. However, the resolution of the 576 nm emission line shown in Figure 3.9 was 24.8 pm giving an experimental resolution of 23265 which is nearly five times higher and near the expected resolving power. One reason the resolution is so much better at 576 nm than 546 nm is placement of a 450 nm long-pass filter in front of the entrance aperture to the SHS. The filter eliminated more off-axis light and blocked the higher orders from the shorter wavelengths from entering the SHS. Another possibility is the intensity of the 546 nm emission is much higher and thus circular fringe patterns caused by etaloning in the beam-splitter have much higher intensity too which causes broadening of the spectral line. Future studies could include addition of a neutral density filter to reduce the intensity of the 546 nm emission to see if the FWHM is improved.

The signal-to-noise ratios (S/N) were calculated by dividing the signal intensity by the average of the baseline noise. The S/N of the higher groove density gratings (75.3) was nearly three times larger than the second order from the lower groove density gratings (28.4) because the first order from the diffraction gratings is the most efficient which can be observed visually and typical efficiency for this type of diffraction grating for the first order is ~70 – 75% with the efficiency dropping sharply to ~5% for the second order.

To show the stability of the SHLS, two more spectra are shown in Figures 3.10 and 3.11 for the 576 nm and 579 nm mercury emission lines which were acquired at two-week intervals. Each spectrum shows similar resolution in the two emission lines despite

the fact the Littrow was shifted between other Littrow settings to measure around 520 nm for copper up to 669 nm to measure lithium.

A copper LIBS measurement was made with Littrow set near 580 nm to verify accuracy and calibration of the micrometer adjusted rotational stage. The spectrum is shown in Figure 3.12. The Cu peak has a resolution of 62 pm which was the highest resolution obtained with LIBS using the SHLS. Due to time constraints further evaluation was not possible.

## 3.3 CONCLUSION

We have shown that a small SHLS, with 25 mm aperture and 600 grooves/mm gratings, has resolution of 58 pm. Although this is not sufficient to resolve U ($^{235}$U/$^{238}$U ~26 pm), Pu ($^{239}$Pu/$^{240}$Pu~ 6 pm), or Li ($^{6}$Li/$^{7}$Li ~15 pm), it does show the potential for a small SHLS to measure isotopes since it is possible to increase the resolving power of the SHS by several factors as demonstrated by Harlander with the Spatial Heterodyne Imager for Mesospheric Radicals (SHIMMER) instrument used for the remote sensing of hydroxyl radicals in the middle atmosphere. [28] It is also possible that spectra measured with the current SHLS can resolve uranium and lithium isotopes using curve fitting algorithms.
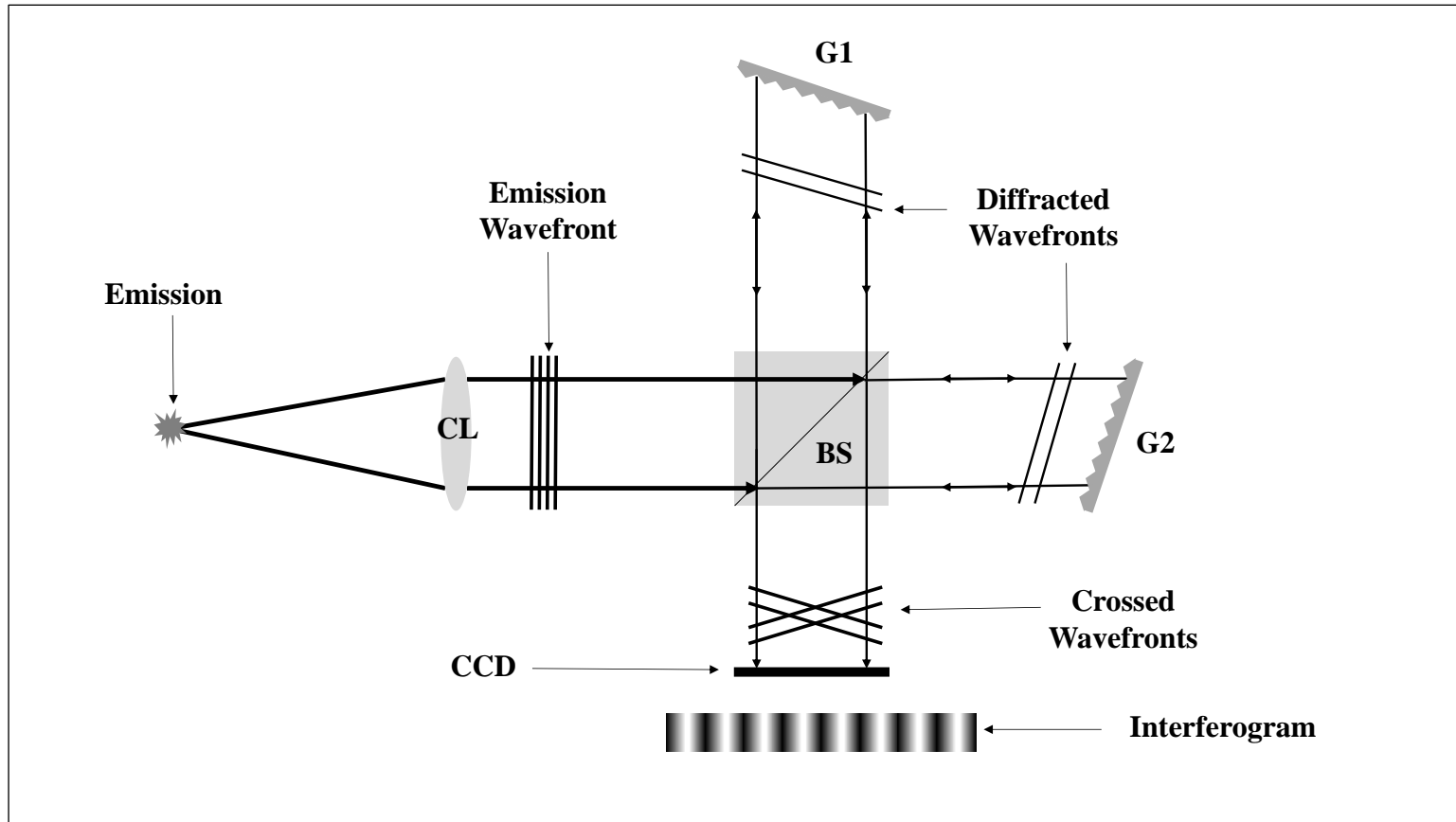
Figure 3.1 Schematic and working principle of the SHS. The basic components of the SHS are the collection lens (CL), beam-splitter (BS), diffraction gratings (G1 and G2), imaging lens (placement shown in Figure 3.2) and the detector (CCD). The diffraction of the heterodyned wavelengths produces crossing wave-fronts at the beam-splitter. The crossing wave-fronts produce wavelength dependent interference patterns imaged onto the CCD.
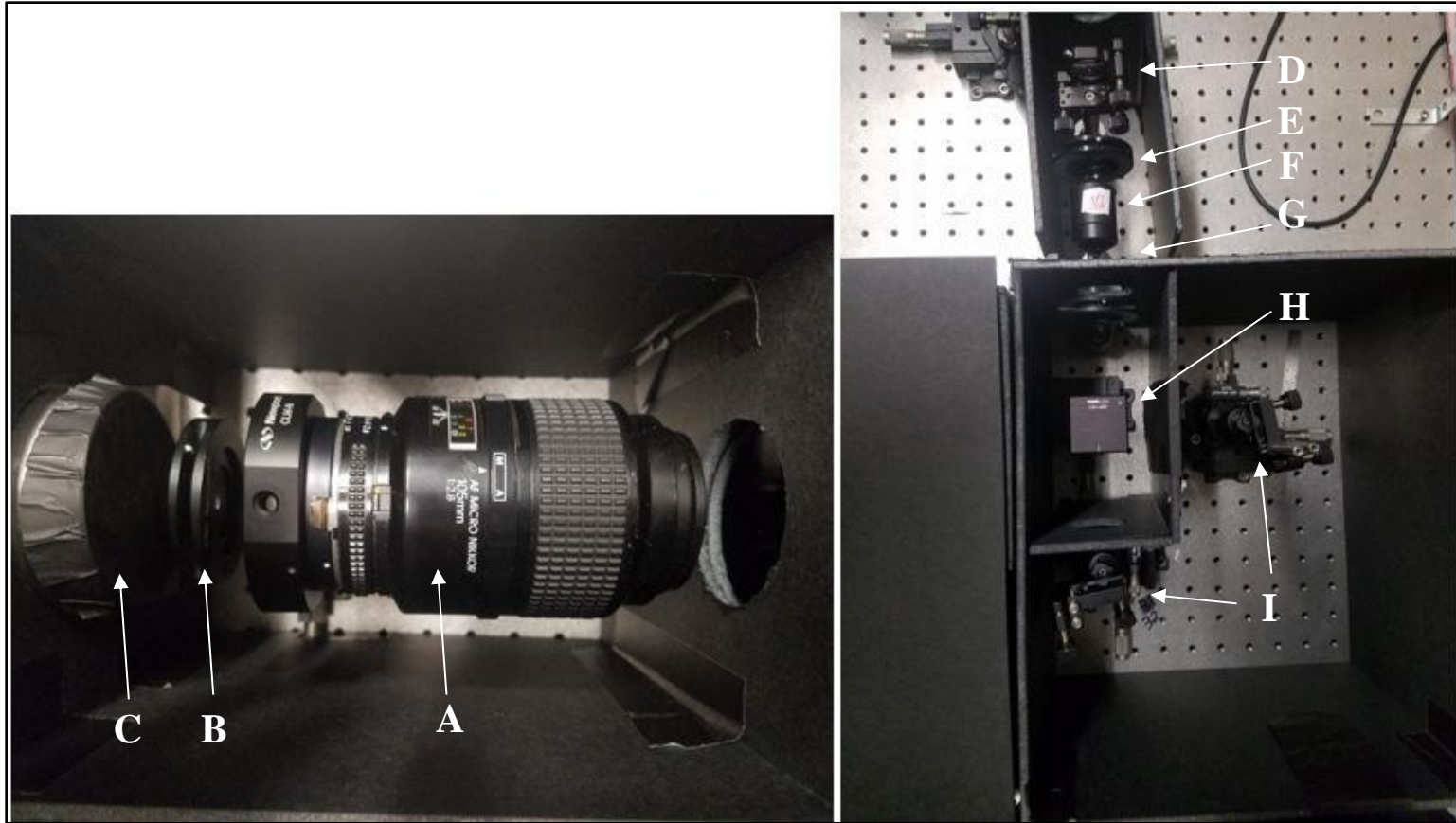
Figure 3.2 The photos show the current SHLS. To the left is the Nikon 105 mm imaging lens (A) with a spatial filter (B) and the PI-MAX iCCD (C) shown to the left of the imaging lens. The photo to the right shows from top to bottom: the f/2 collection lens (D), iris (15 mm opening) (E), 450 nm long pass filter (F), a second iris (15 mm opening) (G), the beam-splitter (H), and the two 600 grooves/mm diffraction gratings (I).
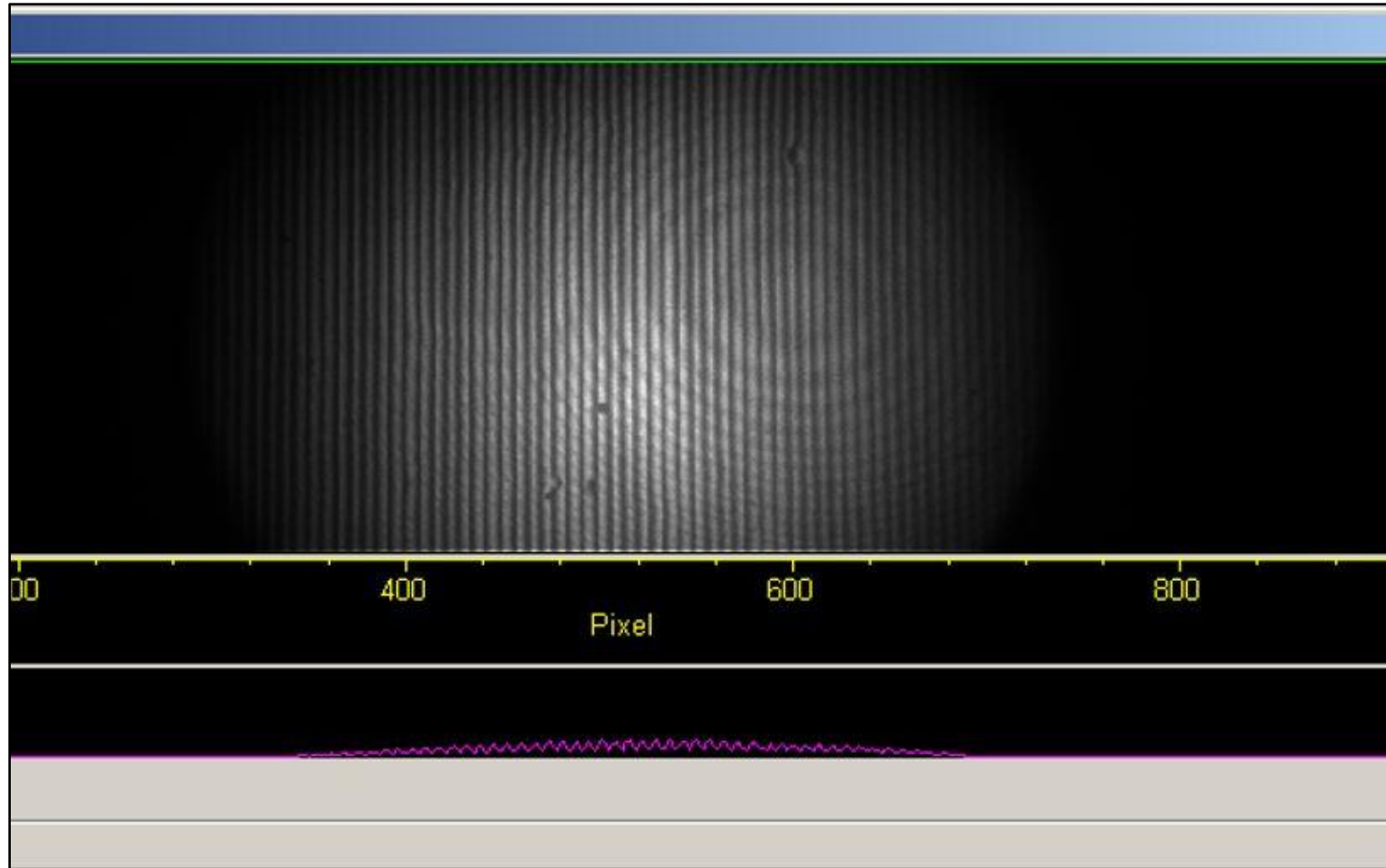
Figure 3.3 The figure shows a screenshot of an interference pattern for the 546 nm elemental mercury emission that can be used to count the number of fringes over a pixel range which can be converted to give the number of fringes/cm used in equation 3.
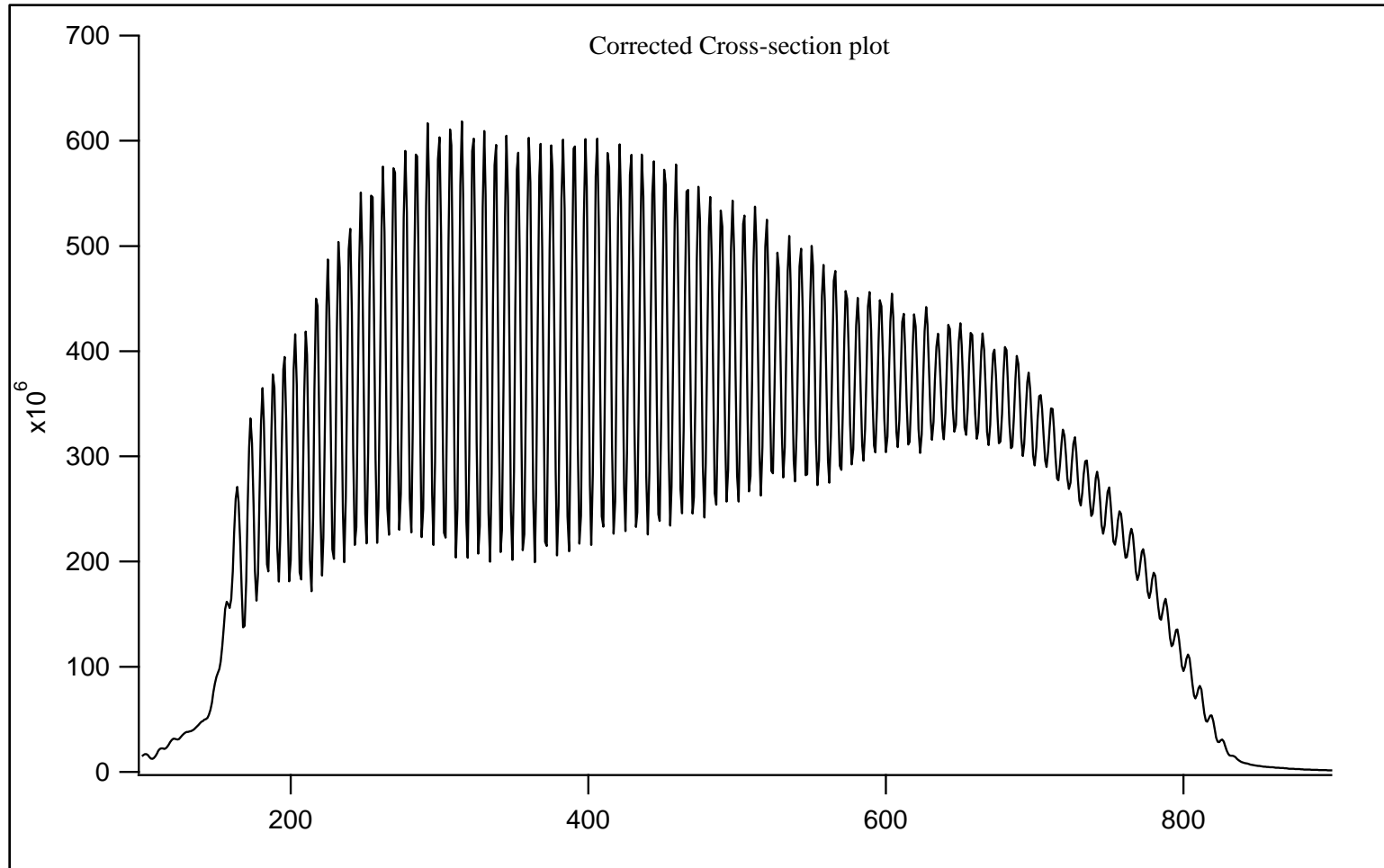
Figure 3.4 Cross-section plot of the interferogram shown in Figure 3.3. Which allows higher accuracy when counting the number of maxima over a specific pixel range to determine the fringes/cm. The y-axis is Intensity and the x-axis is pixel number.
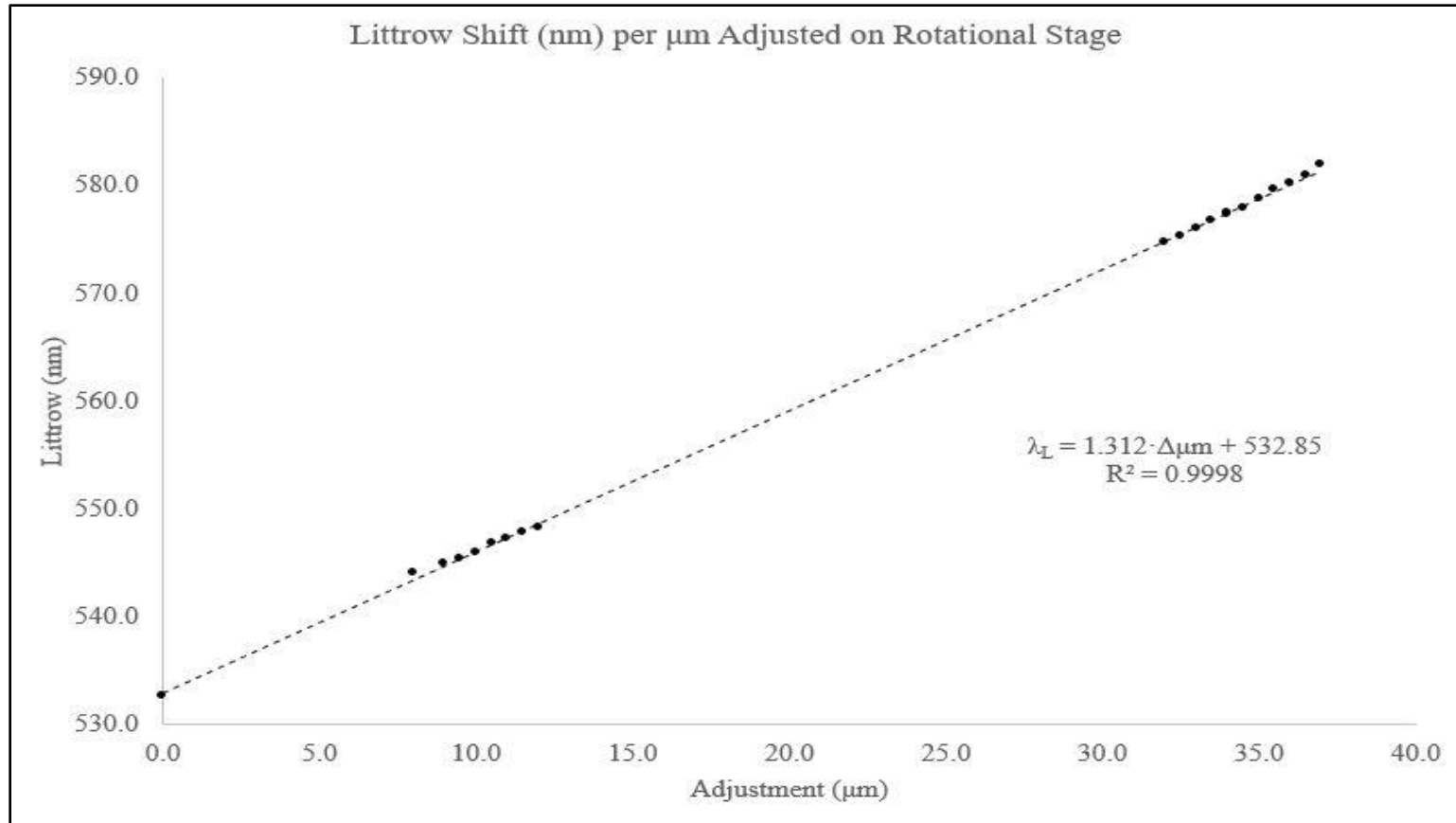
Figure 3.5 The graph above shows the calibration curve and linear regression used to accurately shift Littrow without a monochromatic light source. As can be seen the correlation is very high. The slope was 1.312 ±0.004 nm/μm and the intercept was 532.9 ±0.1 nm.
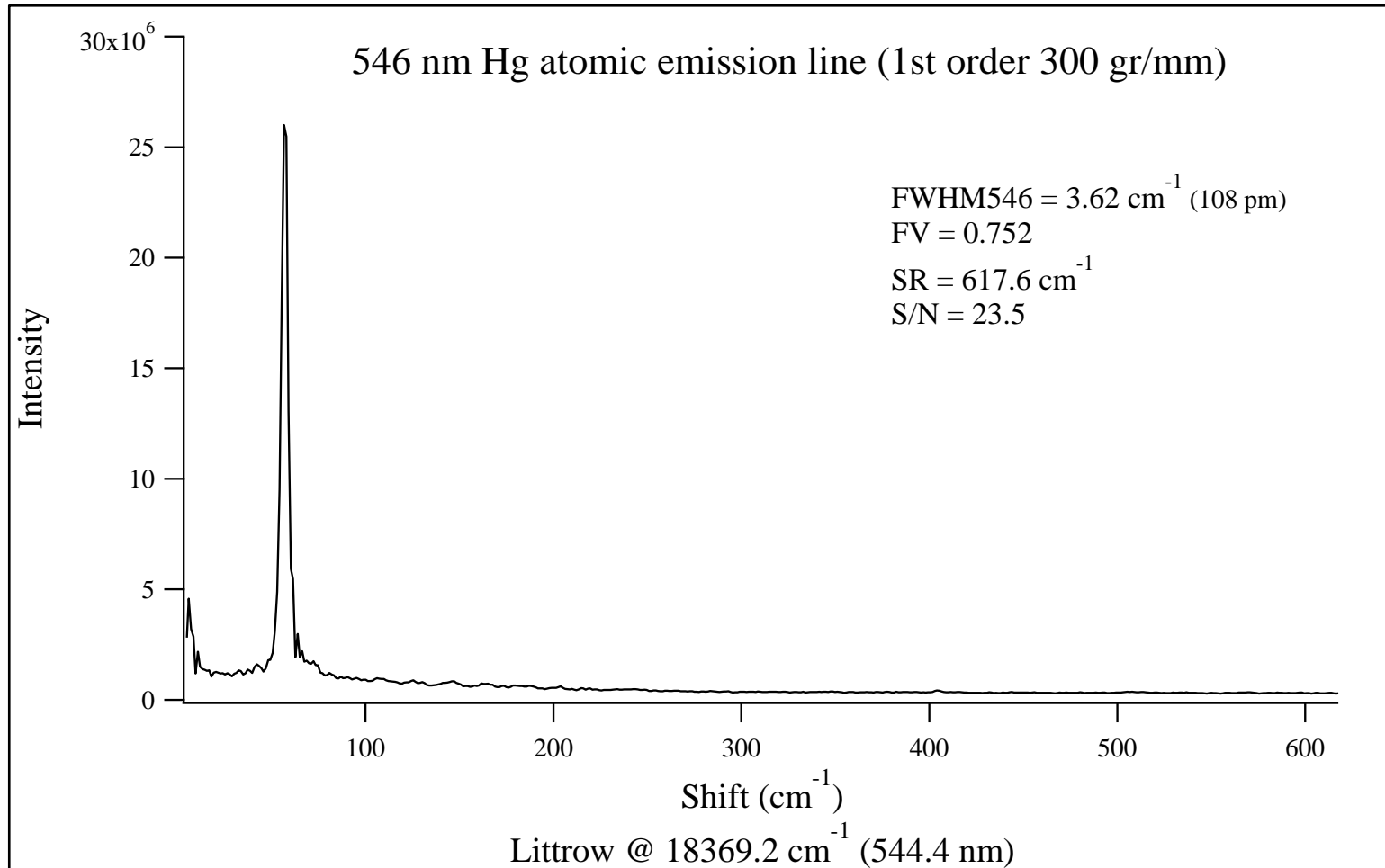
Figure 3.6 spectrum above shows the 546 nm elemental emission line of the mercury reference lamp using the first order of the 300 groove/mm diffraction gratings.
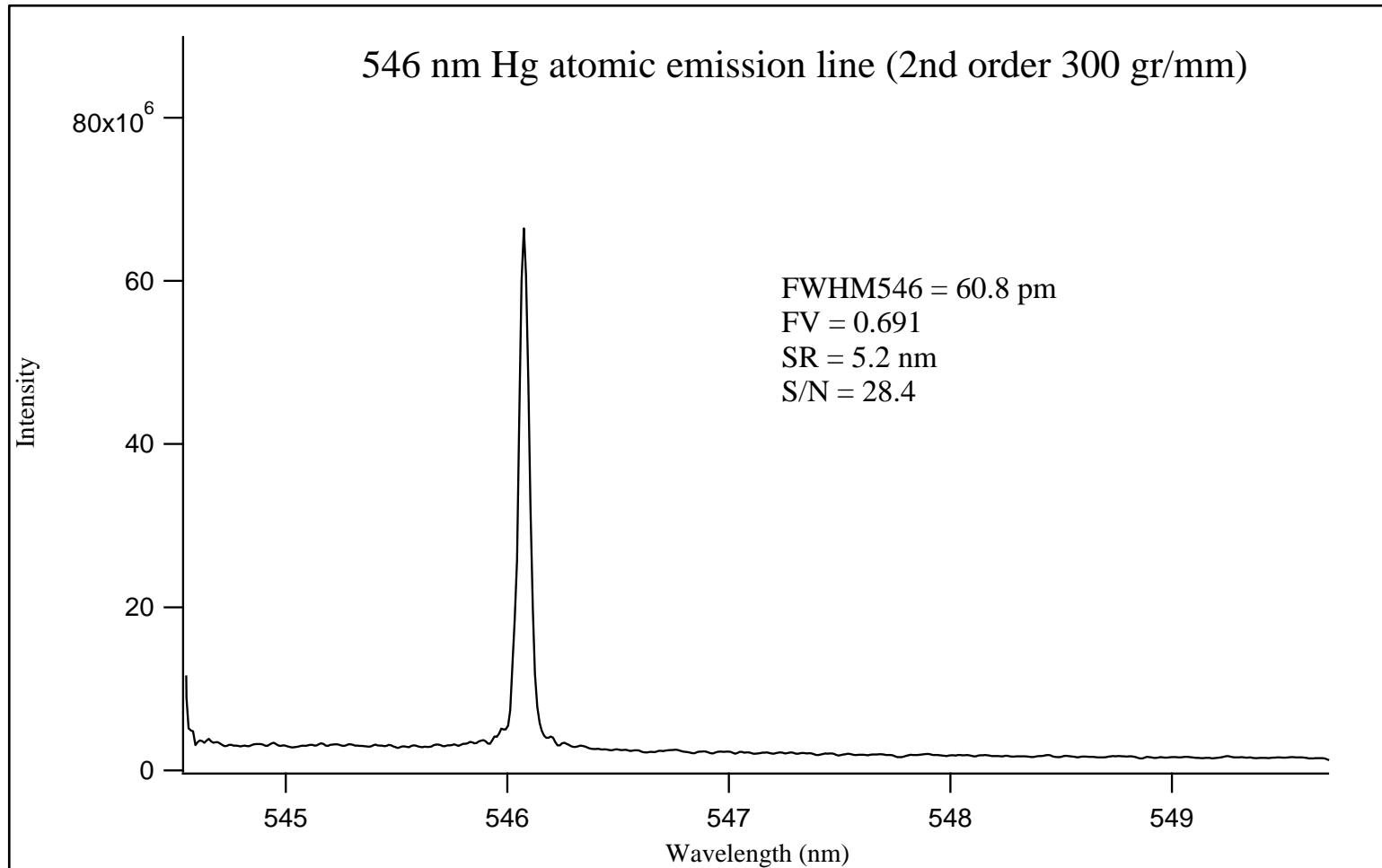
Figure 3.7 The spectrum above shows the 546 nm elemental emission line of the mercury reference lamp using the second order of the 300 groove/mm diffraction gratings.
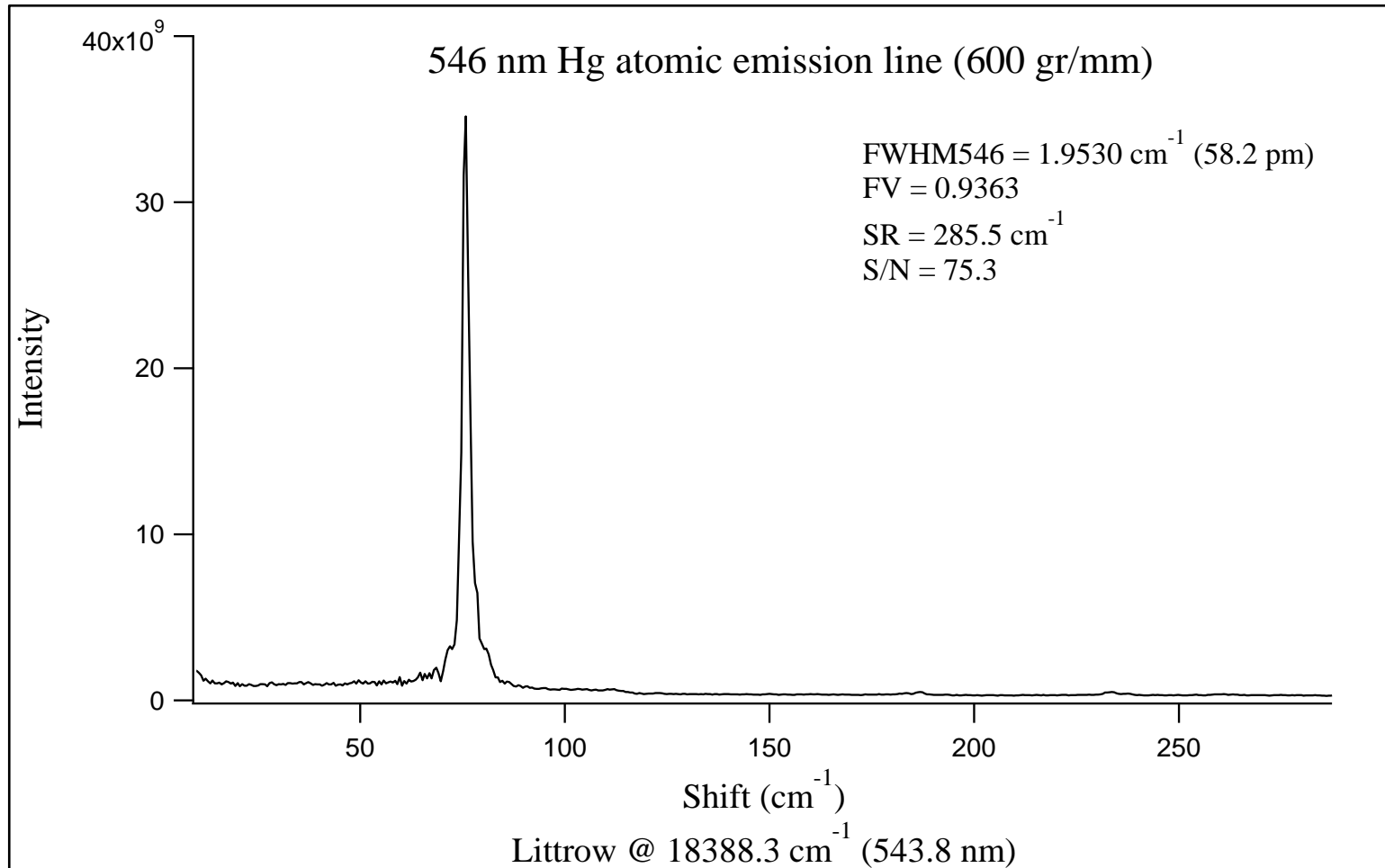
Figure 3.8 This spectrum shows the 546 nm elemental emission line of the mercury reference lamp using the first order of the 600 groove/mm diffraction gratings.
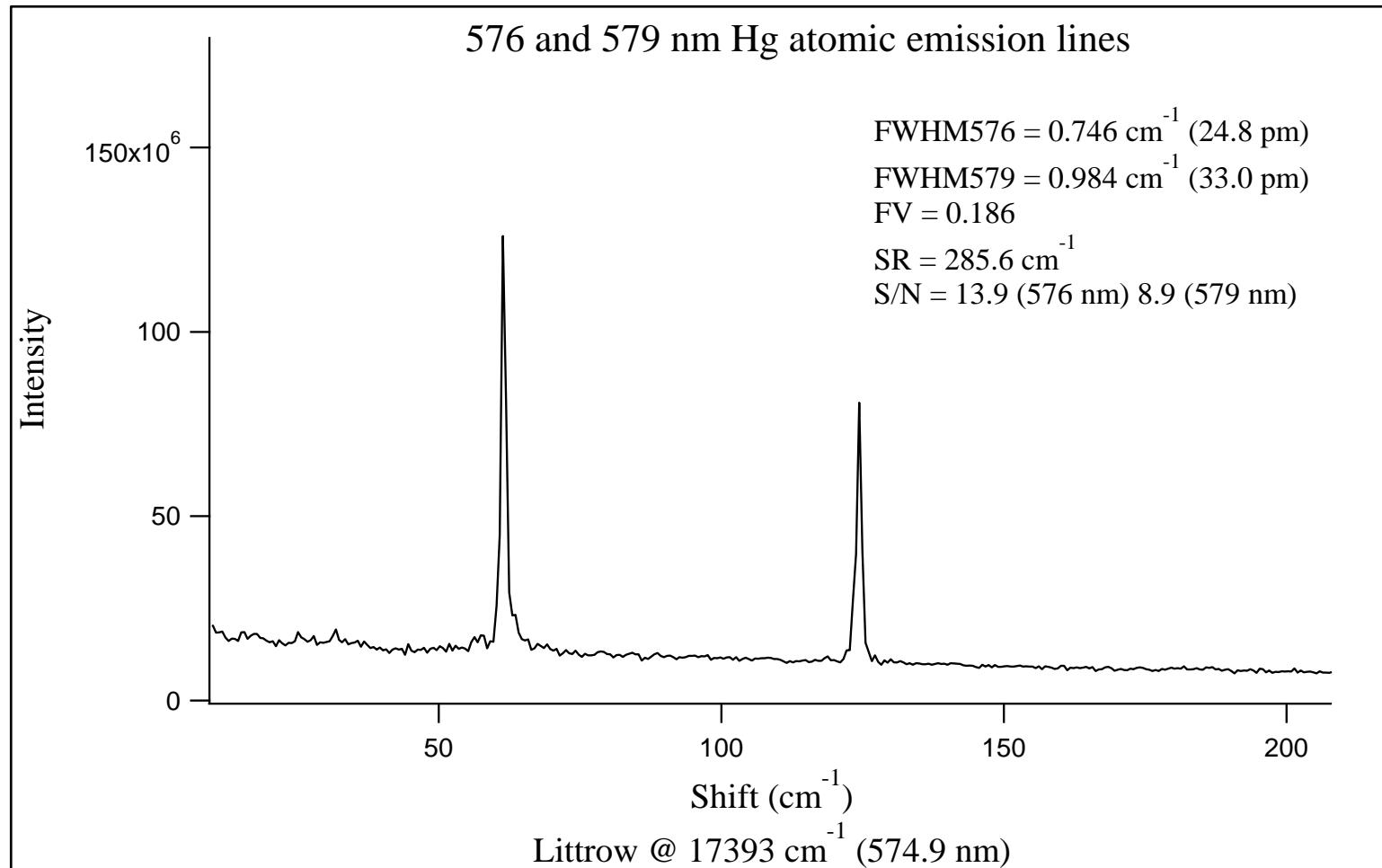
Figure 3.9 This figure shows the spectrum of the 576 nm and 579 nm elemental emission lines of the mercury reference lamp using the first order of the 600 groove/mm diffraction gratings.

Figure 3.10 The spectrum above is a repeat of Figure 3.9 but the measurement was made after Littrow had been shifted back and forth between 520 nm to 669 nm.
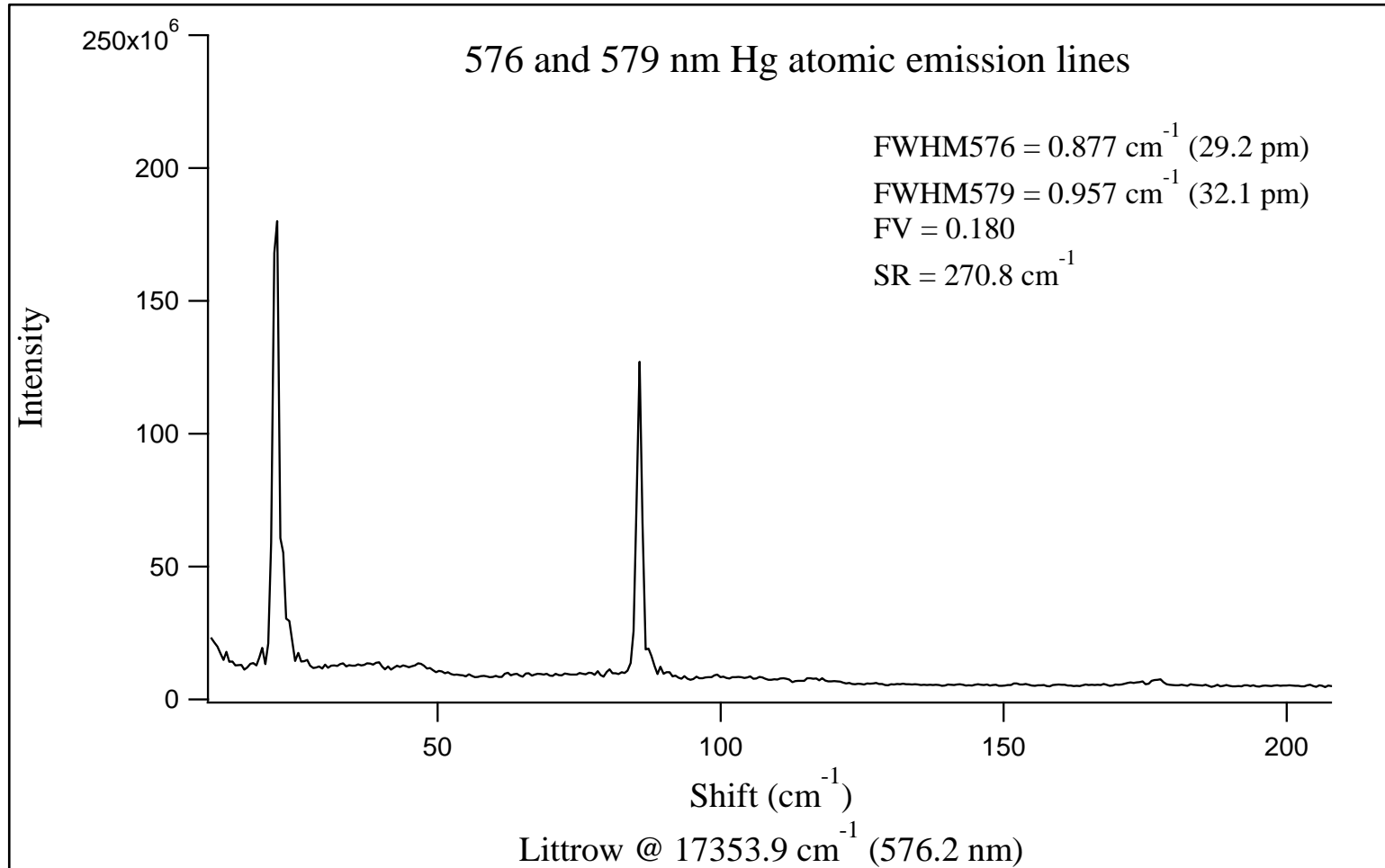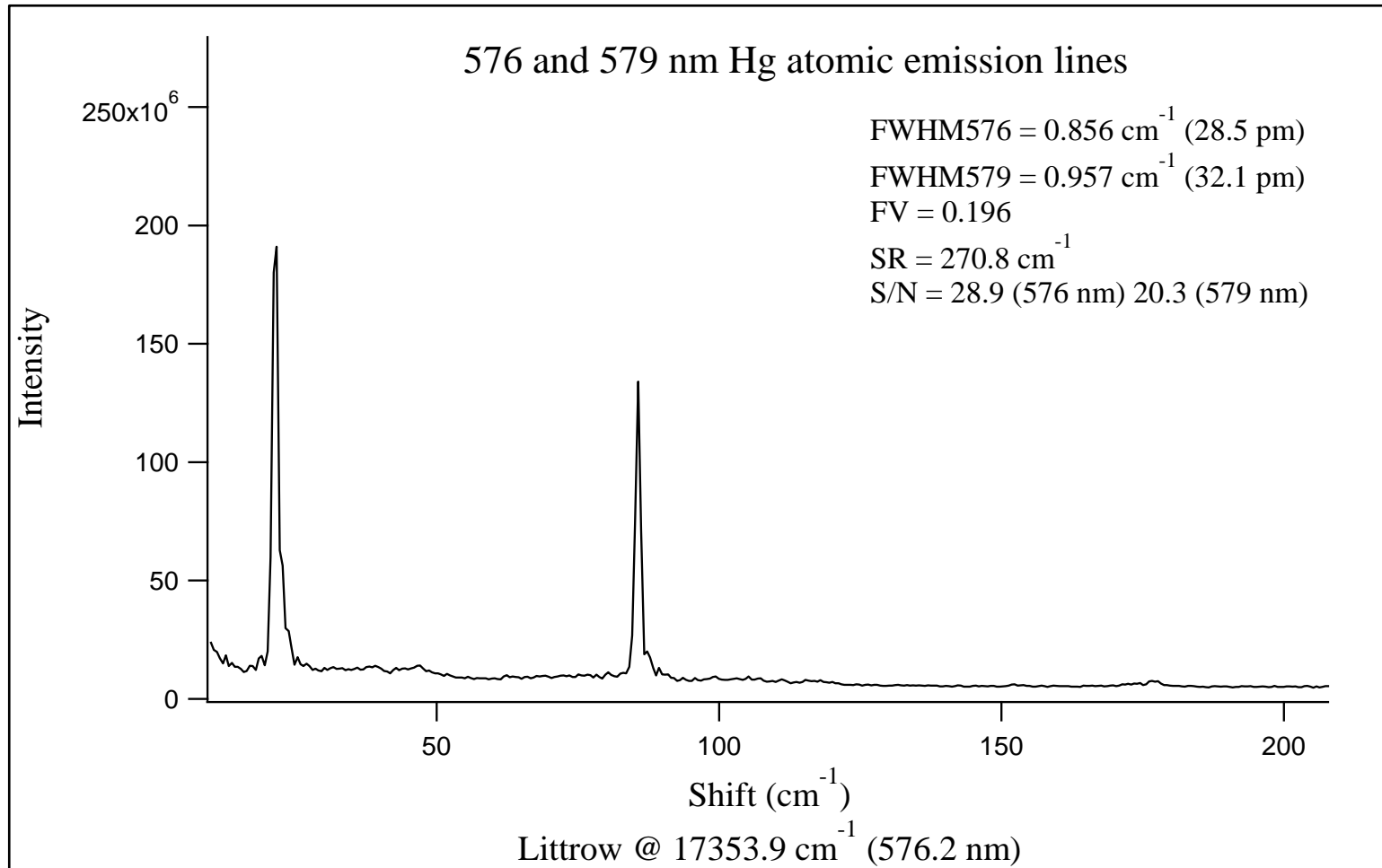
Figure 3.11 The spectrum above is a repeat of Figure 3.9 but the measurement was made two weeks after Littrow had been shifted back and forth between 520 nm to 669 nm.
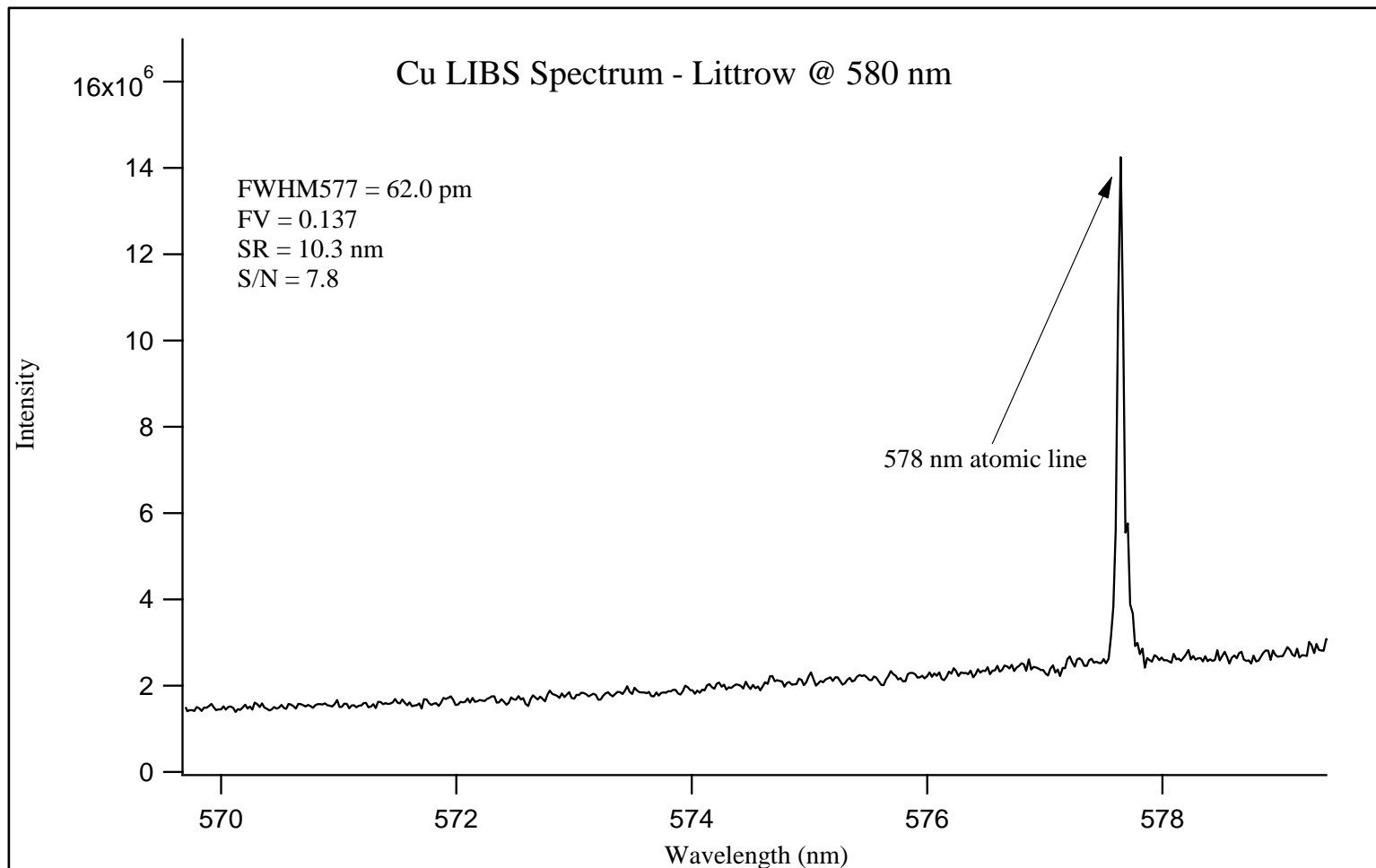
Figure 3.12 The figure shows a copper LIBS spectrum of the 578 nm elemental emission line. The resolution was the best measured with the SHLS so far.

# REFERENCES

(1)     D.A. Cremers and J. Radziemski. "Handbook of Laser-Induced Breakdown Spectroscopy". 2nd Edition. John Wiley & Sons, Ltd. Chichester, West Sussex, UK. 2012.

(2)     D.A. Cremers, A. Beddingfield, R. Smithwick. "Monitoring Uranium, Hydrogen, and Lithium and Their Isotopes Using a Compact Laser-Induced Breakdown Spectroscopy (LIBS) Probe and High-Resolution Spectrometer". Applied Spectroscopy. 2012. 66(3) p. 250-261.

(3)     R. E. Russo, T. W. Suen, A. A. Bol'shakov, J. Yoo, O. Sorkhabi, X. Mao, J. Gonzalez, D. Oropeza, and V. Zorba. "Laser Plasma Spectroscopy". Journal of Analytical Atomic Spectrometry. 2011 26: p. 1596-1603.

(4)     C. López-Moreno, S. Palanco, J.J. Laserna, F. DeLucia Jr., A.W. Miziolek, J. Rose, R.A. Walters, A.I. Whitehouse. "Test of a stand-off laser-induced breakdown spectroscopy sensor for the detection of explosive residues on solid surfaces". Journal of Analytical Atomic Spectrometry. 2006. 21: p. 55-60.

(5)     A.K. Knight, N.L. Scherbarth, D.A. Cremers, M.J. Ferris. "Characterization of Laser-induced Breakdown Spectroscopy (LIBS) for Application to Space Exploration". Applied Spectroscopy. 2000. p. 139-148.

(6)     Gaona, P. Lucena, J. Moros, F.J. Fortes, S. Guirado, J. Serrano, and J.J. Laserna. "Evaluating the Use of Standoff LIBS in Architectural Heritage: Surveying the Cathedral of Malaga". Journal of Analytical Atomic Spectrometry. 2013. 28 p. 810-820.

(7)     J. Moros, J.J. Laserna. "New Raman-Laser-Induced Breakdown Spectroscopy Identity of Explosives Using Parametric Data Fusion on an Integrated Sensing Platform". Analytical Chemistry. 83(16): p. 6275-6285.

(8)     D.W. Hahn and N. Omenetto. "Laser-Induced Breakdown Spectroscopy (LIBS), Part I: Review of Basic Diagnostics and Plasma–Particle Interactions: Still-Challenging Issues Within the Analytical Plasma Community". Applied Spectroscopy. 2010. 64(12) p. 335A – 366A.

(9)     Y. Markushin, A. Marcano, S. Rock, and N. Melikechi. "Determination of Protein Hydrogen Composition by Laser-Induced Breakdown Spectroscopy". Journal of Analytical Atomic Spectrometry. 2010. 25: p. 148-149.

(10)  D'Ulivo, M. Onor, E. Pitzalis, R. Spiniello, L. Lampugnani, G. Cristoforetti, S. Legnaioli, V. Palleschi, A. Salvetti, and E. Tognoni. "Determination of the Deuterium/Hydrogen Ratio in Gas Reaction Products by Laser-Induced Breakdown Spectroscopy". Spectrochimica Acta Part B. 2006. 61: p. 797-802.

(11)  D. E. Spence, P. N. Kean, and W. Sibbett, "60-fsec pulse generation from a self-mode-locked Ti:sapphire laser," Optical Letters. 1991. 16(1) p. 42–44.

(12)  A.J. Kox. "Then & Now: The Discovery of the Stark Effect and Its Early Theoretical Explanations". Annalen der Physik. Berlin. 2013. 525(5) p. A63-A66.

(13)  J. Stark. "Observation of the Separation of Spectral Lines by an Electric Field". Nature. 1913. 97(401) p. 401.

(14)  B. Salle, D.A. Cremers, S. Maurice, R.C. Wiens. "Laser-Induced Breakdown Spectroscopy for Space Exploration Applications: Influence of the Ambient Pressure on the Calibration Curves Prepared from Soil and Clasy Samples". Spectrochimica Acta Part B: Atomic Spectroscopy. 2005. 60(4) p. 479-490.

(15)  S.M. Clegg, R. Wiens, A.K. Misra, S.K. Sharma, J. Lambert, S. Bender, R. Newell, K. Nowak-Lovato, S. Smrekar, M. Darby Dyer, and S. Maurice. "Planetary Geochemical Investigations Using Raman and Laser-Induced Breakdown Spectroscopy". Applied Spectroscopy. 2014. 68(9) p. 925-936.

(16)  R. González, P. Lucena, L.M. Tobaria, J.J. Laserna. "Standoff LIBS detection of explosive residues behind a barrier". Journal of Analytical Atomic Spectrometry. 2009. 24(8): p. 1123-1126.

(17)  V. Lazic, A. Palucci, S. Jovicevic, M. Carapanese, C. Poggi, E. Buono. "Detection of explosives at trace levels by Laser Induced Breakdown Spectroscopy (LIBS)". Chemical, Biological, Radiological, Nuclear, and Explosives (CBRNE) Sensing XI, vol. 7665 of Proceedings of SPIE, April 2010.

(18)  A.J.R. Bauer and S.G. Buckley. "Novel Applications of Laser-Induced Breakdown Spectroscopy". Applied Spectroscopy. 2017. 71(4) p 553-566.

(19)  R. Grönlund, M. Lundqvist, S. Svanberg. "Remote imaging laser-induced breakdown spectroscopy and remote cultural heritage ablative cleaning". Optics Letters. 2005. 30(21): 2882-2884.

(20)  P.D. Barnett, N. Lamsal, and S.M. Angel. "Standoff Laser-Induced Breakdown Spectroscopy (LIBS) Using a Miniature Wide Field of View Spatial Heterodyne Spectrometer with Sub-Microsteradian Collection Optics". Applied Spectroscopy. 2017. 71(4) p. 583-590.

(21)  X. Mao, A. A. Bol'shakov, I. Choi, C. P. McKay, D. L. Perry, O. Sorkhabi, and R. Russo. "Laser Ablation Molecular Isotopic Spectrometry: Strontium and its Isotopes". Spectrochimica Acta Part B. 2011. 66: p. 767-775.

(22)  X. Mao, A. A. Bol'shakov, D. L. Perry, O. Sorkhabi, and R. Russo. "Laser Ablation Molecular Isotopic Spectrometry: Paramenter Influence on Boron Isotope Measurements". Spectrochimica Acta Part B. 2011. 66: p. 604-609.

(23)  E. de Hoffmann and V. Stroobant. "Mass Spectrometry: Principles and Applications". 3rd Edition. John Wiley & Sons, Ltd. Chichester, West Sussex, UK. 2007.

(24)  M. Krachler, R. Alvarez-Sarandes, and G. Rasmussen. "High-Resolution Inductively Coupled Plasma Optical Emission Spectrometry for $^{234}U/^{238}Pu$ Age Dating of Plutonium Materials and Comparison to Sector Field Inductively Coupled Plasma Mass Spectrometry". Journal of Analytical Chemistry. 2016. 88 p. 8862-8869.

(25)  A.A. Bol'shakov, X. Mao, J.J. Gonzalez, and R.E. Russo. "Laser Ablation Molecular Isotopic Spectrometry (LAMIS): Current State of the Art". Journal of od Analytical Atomic Spectrometry. 2016. 31 p. 119-134.

(26)  J.M. Harlander. Spatial Heterodyne Spectroscopy: Interferometric Performance at Any Wavelength without Scanning. [Ph.D. Dissertation]. Madison, Wisconsin: University of Wisconsin-Madison, 1991.

(27)  J.M. Harlander, F.L. Roesler, R.J. Reynolds, K. Jaehnig, W.A. Sanders. "Differential, Field-Widened Spatial Heterodyne Spectrometer for Investigations at High Spectral Resolution of the Diffuse Far Ultraviolet 1548 Å Emission Line from the Interstellar Medium". Proc. SPIE. 1993. 2006. p. 139-148.

(28)  J.M. Harlander, F.L. Roesler, J.G. Cardon, C.R. Englert, and R.R. Conway. "SHIMMER: A Spatial Heterodyne Spectrometer for Remote Sensing of Earth's Middle Atmosphere". Applied Optics. 2002. 41(7) p. 1343-1352.

(29)  N.R. Gomer, C.M. Gordon, P. Lucey, S.K. Sharma, J.C. Carter, and S.M. Angel. "Raman Spectroscopy Using a Spatial Heterodyne Spectrometer: Proof of Concept". Applied Spectroscopy. 2011. 65 p. 849-857.

(30)  I. B. Gornushkin, B. W. Smith, U. Panne, and N. Omenetto. "Laser-Induced Breakdown Spectroscopy Combined with Spatial Heterodyne Spectroscopy". Applied Spectroscopy. 2014. 68(9): p. 1076-1084.